Piezoelectric properties of polyamide 11/NaNbO3nanowire composites

Charlotte David, Jean-Fabien Capsal, Lydia Laffont-Dantras, Eric Dantras, Colette Lacabanne

doi:10.1088/0022-3727/45/41/415305

Piezoelectric properties of polyamide 11/$NaNbO_3$ nanowire composites

Charlotte David[1], Jean-Fabien Capsal[2], Lydia Laffont[3], Eric Dantras[1] and Colette Lacabanne[1]

[1] Physique des Polymères, Institut Carnot CIRIMAT Université Paul Sabatier, 31062 Toulouse, France
[2] LGEF, INSA Lyon, 69621 Villeurbanne, France
[3] MEMO, Institut Carnot CIRIMAT, ENSIACET, 31432 Toulouse, France

E-mail: eric.dantras@univ-tlse3.fr

Abstract

Polyamide 11(PA 11)/sodium niobate nanowire (NW) 0–3 composites with different volume fractions of NWs were synthesized. The electric polarization (P) was measured as a function of the applied electric field (E). The P–E hysteresis loop was used to work out the remanent polarization P_r of these materials. The dielectric permittivity and the piezoelectric strain constant were determined. Good impedance matching between inorganic and organic phases leads to higher electroactivity than conventional lead-free 0–3 composites. The piezoelectric voltage of the PA 11/$NaNbO_3$ NW composites is of the same order as those obtained for fluorinated piezoelectric polymers. These composites could have some applications in flexible, low-cost, environmentally friendly piezoelectric sensors and actuators.

1. Introduction

Over the last few decades, much attention has been paid to the study of organic ferroelectric materials [1–6]. These electroactive polymers are very attractive because of their light weight, easy moulding and good piezo/pyroelectric properties. In sensor applications, the low dielectric properties of polymers enable them to reach a higher piezoelectric sensitivity than those obtained for conventional piezoelectric ceramics. However, to obtain the ferroelectric properties [7, 8], these organic materials require a poling field 10 times higher than conventional ferroelectric ceramics [9, 10]. Consequently, a dielectric breakdown can happen. Moreover, the low thermal stability of the piezoelectric properties of ferroelectric polymers limits their applications [11, 12]. In some particular cases, it is required to preserve the mechanical and easy moulding properties of polymers and the thermal stability of piezoelectric ceramics [13–15]. Many works have reported the elaboration and characterization of polymers/inorganic piezoelectric particle composites [16–22]. The particles studied are synthesized from toxic and non-environmentally friendly precursors (for example PZT) and/or their thermal stability is poor (e.g. $BaTiO_3$, BT). Over the last five years, some ceramic nanowires (NWs) have been synthesized [23–26]. Nevertheless, it appears quite difficult to conserve a non-centrosymmetric crystalline cell that is crucial for ferroelectric activity [27–29]. Recently, Sodano *et al* have shown that the use of piezoelectric NWs instead of particles can lead to an increase in the final piezoelectric properties of composites [30–32].

Here, we report the elaboration and characterization of piezoelectric polyamide 11(PA 11)/sodium niobate (NN) composites. PA 11 is a thermoplastic polymer synthesized from castor oil. NN ceramic has a high piezoelectric activity and a low dielectric permittivity. This ceramic is antiferroelectric from −103 to 370 °C which means this material is characterized by antiparallel alignment of elementary dipoles. They can be induced to be in the ferroelectric phase under a sufficient electric field, which is how NN ceramic can be ferroelectric from 0 to 250 °C [33]. As the melting temperature of the crystalline phase of PA 11 is nearly 200 °C, these composites may possess ferroelectric activity over a wide temperature range. For the sake of simplicity, $NaNbO_3$NWs were chosen.

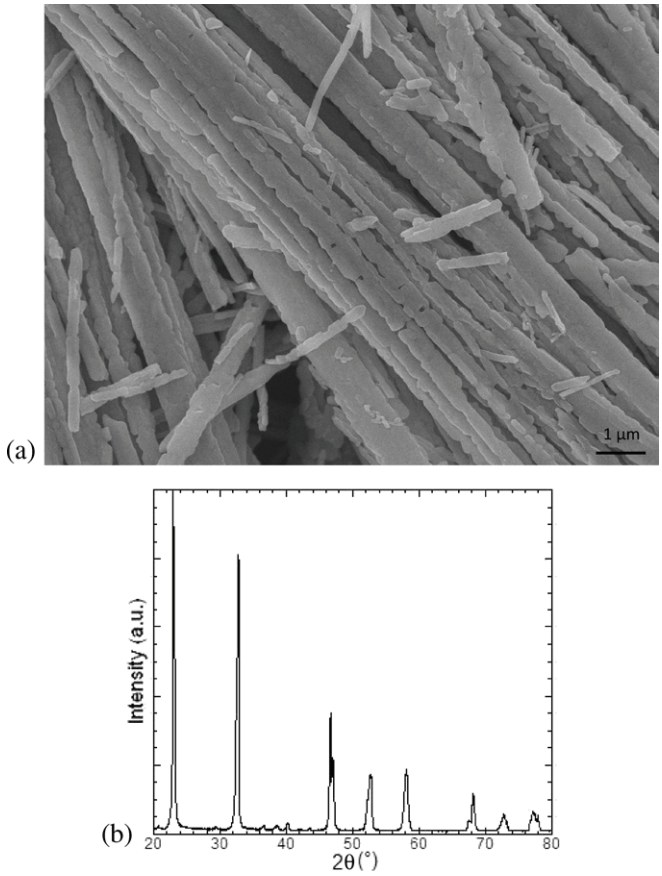

Figure 1. (*a*) Scanning electron microscopy (SEM) image of the as-prepared NN NWs and (*b*) XRD spectra of one set of NN NWs measured at room temperature.

2. Experimental

2.1. Synthesis of NN NWs

NN NWs were synthesized by a hydrothermal reaction between nobium pentoxide (Aldrich) and sodium hydroxide (NaOH, Aldrich). In the first step, niobium pentoxide was dispersed for 5 min in an ultrasonic bath containing a 10M sodium hydroxide solution. Then, the autoclave was filled (filling ratio 50%) with the solution and sealed. The reaction was conducted at 180 °C for 3 h. The white recrystallized precipitate $NaNb_6O_{15}OH$ was recovered, washed several times with deionized water and cured at 600 °C for 6 h in order to obtain $NaNbO_3$. The morphological evolution of the solid products in the reaction at 180 °C has been extensively described in the work published by Zhu *et al* [34]. The fine Nb_2O_5 powder first aggregates to irregular bars, and then niobate fibres with an aspect ratio of hundreds form. The fibres are a metastable intermediate of this reaction, and they completely convert to the final product, $NaNbO_3$ cubes, in the prolonged reaction.

Figure 1(*a*) presents the NN NW morphology determined by a JEOL JSM 6700F scanning electron microscope (SEM). These elaborated NN NWs have a diameter ranging from 500 nm to 1 μm and a length of 50 to 100 μm. The crystalline structure of the NWs was revealed by x-ray diffraction (XRD) at ambient temperature. A Rigaku diffractometer equipped with Cu K_α radiation ($\lambda = 1.5406$ Å) was used. The diffraction pattern was measured in steps of 0.02 s for 1 s in the 20°–80° 2θ range. The FullProf suite of the WinPlotR software was employed to carry out refinements of the diffraction patterns. Figure 1(*b*) shows the XRD pattern of the elaborated NWs. The XRD pattern was indexed as an orthorhombic structure with a space group of *Pbma*, as reported by the JCPDS card No 89-8957 of the $NaNbO_3$ material (atomic ratio Na/Nb close to 1). No crystalline impurities were detected on the diffractogram according to the resolution limit of the x-ray diffractometer. As the electroactivity of inorganic ceramics depends on a non-centrosymmetric crystalline structure (as orthorhombic crystalline structure), NN NWs are supposed to be ferroelectric at room temperature. Nevertheless, the size of NN NWs is critical. The NN NWs must have at least one submicrometre length to prevent sedimentation during the composite processing and this length should not be too small to maintain the non-cubic crystalline structure.

2.2. Elaboration of PA 11/NN NW composites

PA 11/NN composites were elaborated in solution; the processing schematic diagram of figure 2 displays the experimental protocol. PA 11 was dissolved in dimethyl acethyl amide (DMAc). The required weight of NN NWs was introduced and the solution was submitted to ultrasound for 5 min. The solution was filtered, washed with deionized water and the elaborated powder was put into an oven heated at 130 °C in order to evaporate the residual solvent. The polymeric matrix was filled with volume fractions ranging from 10% to 30%. The low volume fraction enables the polymer to preserve its flexibility and light weight. Composite films were prepared by hot pressing the elaborated powder at 220 °C, above the polyamide melting temperature. The thickness of the pressed films was nearly 100 μm. For the poling procedure, gold ink electrodes with a diameter of 2 cm were painted on both sides of the samples in order to homogeneously disperse the electrical charges at the surface. Considering the manufacturing variability of the process, the experiments described below were carried out with three different samples.

2.3. Differential scanning calorimetry

Differential scanning calorimetry (DSC) measurements were performed using a DSC/TMDSC 2920 setup. The sample temperature was calibrated using the onset of melting of tin ($T_m = 231.88$ °C) and indium ($T_m = 156.6$ °C) with a heating rate of $q_h = +5\,^\circ\mathrm{C\,min^{-1}}$. The heat flow was calibrated with the heat of fusion of indium ($\Delta H = 28.45\,\mathrm{J\,g^{-1}}$), and its baseline was corrected with sapphire. DSC experiments were systematically carried out over a temperature range from the equilibrium state $T_{eq} = T_m + 20\,^\circ\mathrm{C}$ down to the glassy state $T_0 = T_g - 70\,^\circ\mathrm{C}$ with a constant cooling rate $q_c = -20\,^\circ\mathrm{C\,min^{-1}}$, and followed by a linear heating rate $q_h = +10\,^\circ\mathrm{C\,min^{-1}}$. For each sample, the glass transition temperature and the specific heat capacity were measured by DSC during a heating scan.

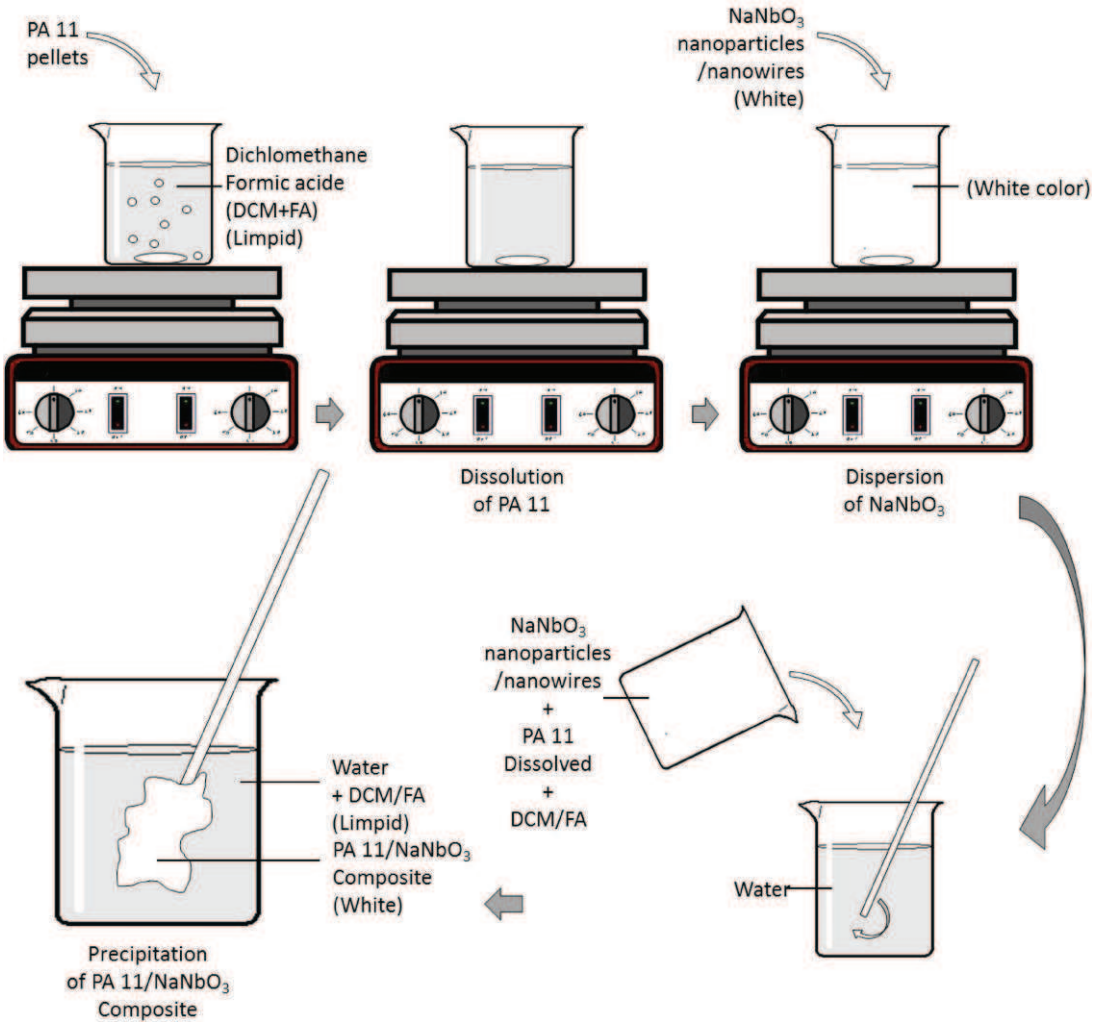

Figure 2. Schematic process of the elaboration of PA 11/NN composites.

2.4. Dielectric spectroscopy

Dynamic dielectric spectroscopy (DDS) was performed using a BDS400 covering a frequency range of 10^{-2}–3×10^{6} Hz with 10 points per decade. Dielectric isotherm spectra were measured. Before each frequency scan, the temperature was kept constant at $\pm0.2\,^{\circ}$C. The real ε'_T and imaginary ε''_T parts of the relative complex permittivity ε^*_T were measured as a function of frequency f, at a given temperature T.

2.5. Poling procedure

The poling procedure allows us to orient the NW dipoles and to obtain a macroscopic polarization P for the composite.

- *Hysteresis measurements.* Hysteresis measurements were performed at room temperature (below the matrix glass transition T_g) in order to minimize the matrix conductivity. A 10 s periodic sinusoidal signal was produced by a ±10 V generator and then amplified using a $\times2000$ V amplifier. During loops, current versus applied field was measured and the macroscopic polarization was calculated.
- *Static polarization.* The final piezoelectric properties of the composites were obtained by poling the samples at 130 °C under a static electric field of 10 kV mm^{-1} for 10 min. This high poling temperature permits one to increase the local field applied to the NWs. As a consequence, the field required to maximize the orientation of the inorganic dipoles in the composite was close to the bulk $NaNbO_3$coercitive field ($\sim$10 kV mm^{-1}) [35]. The electric field was turned off and the samples were short-circuited for 1 day before piezoelectric measurements.

2.6. Piezoelectric measurements

Piezoelectric measurements were carried out using a PM 200 piezometer supplied by Piezotest, UK, with a strength of 0.25 N at a frequency of 110 Hz.

3. Results and discussion

Figure 3 shows a set of thermal analysis curves for the PA 11/NN NW composites with various volume fractions of inorganic NWs. During the second heating run, two endothermic peaks characteristic of PA 11 melting are observed near 184 °C and 189 °C, respectively. These two

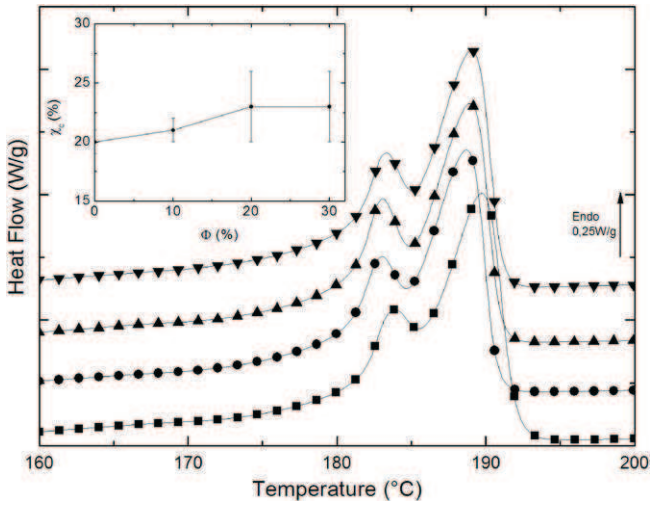

Figure 3. DSC thermograms of the PA 11/NN composites versus volume fraction of the inorganic phase. The inset shows the influence of the inorganic NW volume fraction on the PA 11/NN NW's crystallinity rate: ■, PA 11; ●, PA 11/NN 10% vol; ▲, PA 11/NN 20% vol; ▼, PA 11/NN 20% vol.

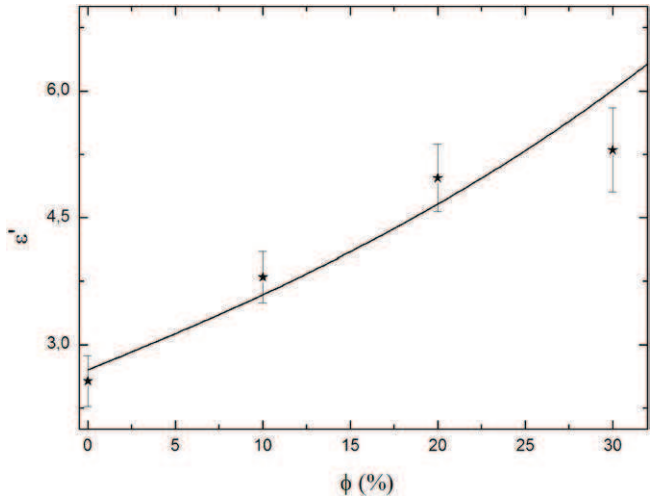

Figure 4. Influence of the volume fraction of inorganic NWs on the real part of the dielectric permittivity $\varepsilon\prime$ of the PA 11/NN NW composites measured at 100 Hz and 25 °C.

peaks are associated with different crystallites of the organic phase; the most stable crystallites correspond to the melting peak with the highest temperature. The melting peaks of the composites are not dependent on the inorganic NWs volume fraction, as shown by the inset in figure 3 where the NW's volume fraction is plotted versus matrix crystallinity. The crystallinity rate χ_c deduced from the melting peak is equal to 20%: its variation is negligible since, in PA 11, the dense hydrogen bond network maintains the crystallinity rate quasi-constant.

Figure 4 shows the real part of the permittivity of PA 11/NN NW composites measured at 100 Hz and 25 °C versus the volume fraction (labelled ϕ of the inorganic NWs). PA 11 has a low dielectric permittivity near 2.6 at 100 Hz. The dielectric permittivity of the composite increases with the volume fraction of the NWs. For 30% of volume fraction, the dielectric permittivity of the composite is twice higher than

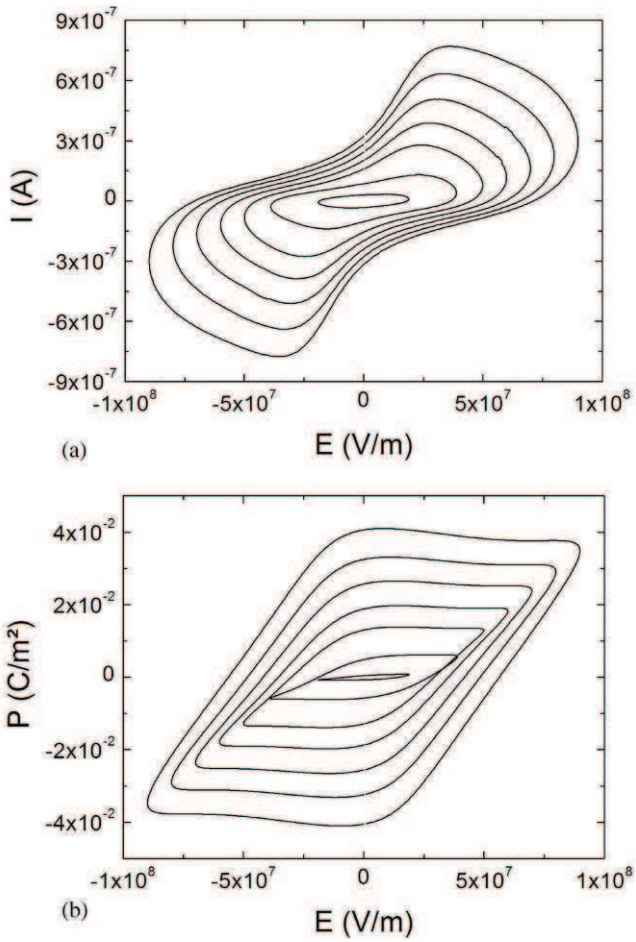

Figure 5. I–E curves (a) and P–E hysteresis loops (b) of the PA 11/NN NW composite with $\phi = 30\%$ measured at room temperature under a sinusoidal electric field.

PA 11. The experimental data are fitted with the effective medium model [36] using the following equation (1):

$$\frac{\varepsilon_{\text{eff}} - \varepsilon_{\text{m}}}{\varepsilon_{\text{eff}} + 2\varepsilon_{\text{m}}} = \phi \frac{\varepsilon_{\text{incl}} - \varepsilon_{\text{m}}}{\varepsilon_{\text{incl}} + 2\varepsilon_{\text{m}}}, \tag{1}$$

where ε_{eff}, ε_{m} and $\varepsilon_{\text{incl}}$ are the real part of the dielectric permittivity of the composite, matrix and NN NWs, respectively.

Using the effective medium model (equation (1)), we can extract the dielectric permittivity of the NN at 25 °C and 100 Hz. The dielectric permittivity of NN (labelled ε_c) is found to be equal to 200 which is in good agreement with the values reported in the literature [37]. This result confirms the good crystallinity of the ferroelectric particles.

Figures 5(a) and (b) show the I–E curves and P–E hysteresis loops of the composites with a volume fraction of 30%. Measurements were performed at room temperature on a 63 μm thick film with 9 mm^2 poling area. As a sinusoidal electric field with a period of 10 s was applied on the sample, the current (I) in the external circuit is the summation of two currents: the displacement current based on the polarization and capacitance, and the conduction current according to

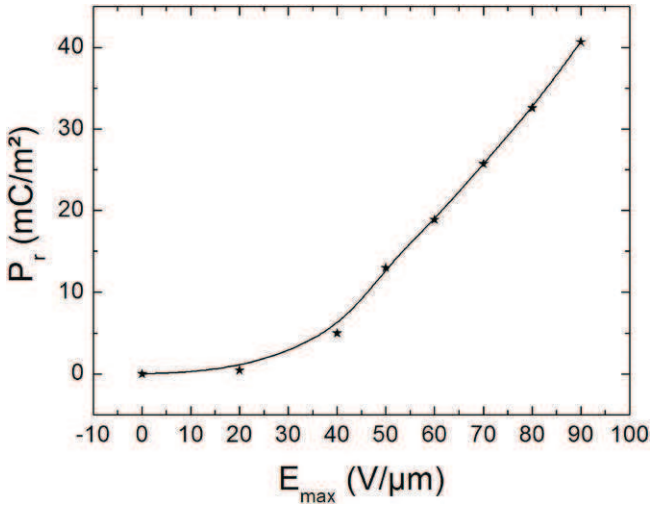

Figure 6. Remanent polarization P_r of the PA 11/NN NW composites with $\phi = 30\%$ versus the maximum value of the applied sinusoidal electric field.

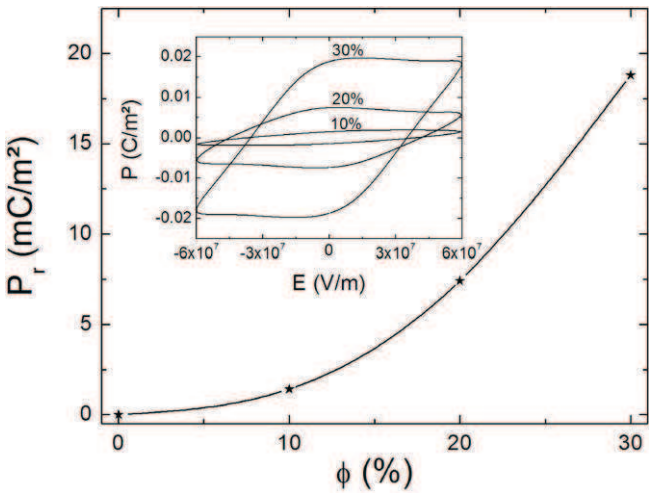

Figure 7. Remanent polarization P_r at $E = 60\,\mathrm{kV\,mm^{-1}}$ versus the volume fraction of inorganic NWs. The inset shows the P–E hysteresis loops of the PA 11/NN NW composites with $\phi = 10\%$, 20%, 30% measured at room temperature, under a sinusoidal electric field.

equation (2):

$$I = I_d + I_R = \frac{dP}{dt} + \varepsilon\varepsilon_0\frac{dE}{dt} + \frac{E}{R}, \tag{2}$$

where I is the poling current, I_d is the displacement current, I_R is the conduction current, P is the polarization, ε is the relative dielectric permittivity, ε is the permittivity of vacuum, E is the applied electric field and R is the electrical resistance.

Thus, using equation (2), the P–E hysteresis loop was calculated after subtraction of the resistance and capacitance terms. As the electric field is increased, a shoulder appears on the I–E signal (figure 5(*a*)); it indicates the ferroelectric behaviour of this material. The increase in the ferroelectric behaviour is pointed out on the P–E hysteresis loops (figure 5(*b*)) by the increase in the remanent polarization of the sample with E. Figure 6 reports the remanent polarization values as a function of the maximal value of the external electric field for each loop. No evident influence of the ferroelectric NWs was found below $E = 20\,\mathrm{kV\,mm^{-1}}$. For a higher applied electric field, a significant increase in the remanent polarization of the composite was shown indicating a progressive orientation of the dipoles of the inorganic phase. For an electric field of $90\,\mathrm{kV\,mm^{-1}}$, the remanent polarization was nearly $40\,\mathrm{mC\,m^{-2}}$. No saturation of the ferroelectric behaviour was pointed out at room temperature, even for very high applied electric fields. It is mainly due to the relative values of the low dielectric permittivity of the polymer and the high dielectric permittivity of the ceramic NWs; all the dipoles of the inorganic phase were not oriented. The local electric field E_c really seen by the ferroelectric NWs [38] is given by

$$E_c = \frac{3\varepsilon}{3\varepsilon + \varepsilon_c}E_0 = L_E E_0, \tag{3}$$

where E_0 is the electric field applied to the composite and ε is the relative dielectric permittivity of the composite ($\varepsilon = 5$). As the coercitive field of the NN ceramic is nearly $10\,\mathrm{kV\,mm^{-1}}$, we can extract from equation (3) the field required to orient all the dipoles of the ceramic phase at room temperature. This required electric field, to reach the maximal ferroelectric state at room temperature, is $143\,\mathrm{kV\,mm^{-1}}$. Due to electrical breakdown, it was not possible to apply such an elevated electric field to the sample, indicating that a room temperature poling procedure does not enable efficient ferroelectric behaviour of the composites.

Figure 7(*a*) shows the P–E hysteresis loops of PA/NN NW composites measured at room temperature under a sinusoidal electric field of $60\,\mathrm{kV\,mm^{-1}}$ with a period of 10 s. The values of the remanent polarization of the composites versus the volume fraction of the inorganic phases are reported in figure 7(*b*). As the volume fraction increases, a non-linear increase in P_r is shown. The remanent polarization of the composites increases from $1.5\,\mathrm{mC\,m^{-2}}$ for a volume fraction of 10% to $19\,\mathrm{mC\,m^{-2}}$ for a volume fraction of 30%. It is evident from these curves that the electroactive properties of these materials increase with the volume fraction of the inorganic phases.

Prior to the piezoelectric measurement, the samples should be poled in order to orient the dipoles of the inorganic phase and to get a macroscopic polarization of the samples. This poling process is realized at a high temperature in order to reach a saturated ferroelectric state. The optimized poling process used for the samples is a poling field applied for 10 min at 130 °C ($T > T_g$ polymer). At this temperature, the Maxwell–Wagner–Sillars relaxation associated with the heterogeneities of the polymeric matrix is responsible for the 'apparent' high dielectric permittivity at a low frequency. During the poling process, a good impedance matching between the inorganic and organic phases is reached. The electric field applied to the composite is close to the local electric field seen by the particles. As a consequence, the necessary field for poling the NN NWs becomes close to the coercitive field of the NN bulk. Then, the saturation of the piezoelectric effect is obtained for an applied electric field $E = 10\,\mathrm{kV\,mm^{-1}}$. The final piezoelectric activity is

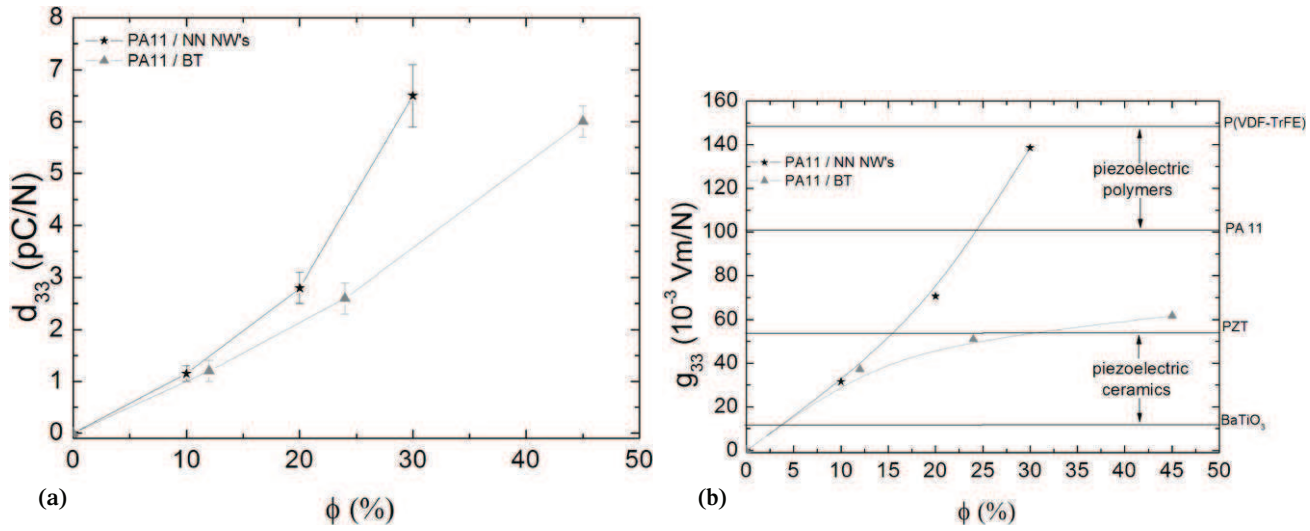

Figure 8. Piezoelectric strain constant d_{33} (a) and piezoelectric voltage constant g_{33} (b) of the PA 11/NN NW composites and PA 11/$BaTiO_3$ particle composites versus the volume fraction of the inorganic phase.

characterized by the piezoelectric strain constant measured in the direction of the poling field. Figure 8(a) presents the piezoelectric strain constant d_{33} recorded at 100 Hz and 25 °C, versus the volume fraction of the inorganic particles. The evolution of d_{33} with volume fraction for the PA 11/NN NW composites is similar to the evolution of P_r. These results are consistent with the fact that d_{33} is due to the variation of P_r submitted to the dynamic mechanical load. d_{33} increases from 1 pC N^{-1} for a volume fraction of 10% to 6.5 pC N^{-1} for $\phi = 30\%$. A literature survey shows that this value is comparable to that of a polymer/PZT composite [39]. It is important to emphasize that the elaboration of the NN NWs do not require a toxic precursor as in the case of commonly used piezoelectric ceramics (PZT, $BaTiO_3$, etc).

The piezoelectric constant of the PA 11/NN NW composites is compared with d_{33} of PA 11/$BaTiO_3$ nanoparticle composites [21]. $BaTiO_3$ (BT) is a ferroelectric ceramic with a high d_{33} of nearly 110 pC N^{-1} and a very high dielectric permittivity of 1500. This ceramic is twice as piezoelectric as NN ($d_{33} = 50$ pC N^{-1} [33]) and has a dielectric permittivity 7.5 times higher. However, the final piezoelectric activity of the composites made with NN NWs is more important than PA 11/BT composites. For a volume fraction of 30%, d_{33} of the NN NW composites made is twice that of the BT particle composites. This indicates that it is possible to obtain more environmentally friendly composites with high piezoelectric activity.

Figure 8(b) shows the piezoelectric voltage constant g_{33} of either PA 11/BT or PA 11/NN NW composites as a function of the volume fraction of the ceramic particles. g_{33} represents the voltage generated on each side of the sample when it is submitted to a mechanical load according to

$$\Delta V = g_{33} X_3 e, \tag{4}$$

where ΔV is the voltage generated, X_3 is the load applied in the thickness of the sample and e is the thickness of the composite layer and $g_{33} = d_{33}/\varepsilon'$.

From equation (4), the voltage generated by the piezoelectric effect on a 100 μm-thick composite with 30% of NN NWs submitted to a 1 N cm^{-2} load is equal to 140 mV.

As previously described [21], the g_{33} value of the PA 11/BT composite levels off at a volume fraction of 30%. The value of g_{33} for this composite is higher than those obtained for the conventional piezoelectric ceramic. However, the high increase in PA 11/BT dielectric permittivity (due to the very high dielectric permittivity of the BT ceramic) with volume fraction is responsible for the saturation of g_{33} and leads to composites that are less sensitive than piezoelectric polymers. In the case of PA 11/NN NWs, the better impedance matching between ceramic and polymer leads to an optimized ratio between d_{33} and ε' that is responsible for the non-saturation of g_{33}. The final piezoelectric sensitivity of the PA 11/NN NWs with a volume fraction of 30% is in the same range as the piezoelectric sensitivity of the polymer and close to that of P(VDF-TrFE), which is the most sensitive piezoelectric polymer. This figure clearly shows that it is possible to use flexible and environmental friendly materials for sensor use.

4. Conclusion

Highly crystalline sodium niobate nanowires (NN NWs) were synthesized by the hydrothermal method. XRD study of these NWs revealed a high crystallinity and an orthorhombic crystalline structure. This non-centrosymmetric crystalline structure is responsible for the ferroelectric behaviour of these NWs. PA 11/NN NW composites with different volume fractions were elaborated. The poling conditions were determined in order to elaborate the optimized poled ceramic/unpoled polymer composites. We found that the piezoelectric coefficient is highly poling temperature- and time-dependent. By poling the samples above the glass transition of the matrix, the maximum piezoelectric coefficient of the composite was reached in 10 min. The magnitude of the poling field (10 kV mm^{-1}) is analogous with the one used for NN ceramics; i.e. significantly lower than for piezoelectric

polymers (100 kV mm^{-1}). The optimum piezoelectricity is 6.5 pC N^{-1} for the PA 11/NN NWs (volume fraction of 0.3). The piezoelectric activity of the composite was compared with that of PA 11/$BaTiO_3$ composites. The piezoelectric activity of the PA 11/NN NWs is higher than that of the PA 11/$BaTiO_3$ composites. These composites have a piezoelectric activity close to PZT/polymer composites but are lead-free. In sensor use, the piezoelectric voltage of the PA 11/NN NWcomposites was found to be of the same order as that of piezoelectric polymers. However, the high Curie temperature of the NN NWs and the high melting temperature of PA 11 led to composites with higher thermal stability of piezoelectric activity than piezoelectric polymers, up to 180 °C.

References

[1] Kawai H 1969 *Japan. J. Appl. Phys.* **8** 975–6
[2] Samara G A and Bauer F 1992 *Ferroelectrics* **135** 385–99
[3] Lee J S, Prabu A A and Kim K J 2010 *Polymer* **51** 6319–33
[4] Tsutsumi N and Yamaoka T 2009 *Thin solid films* **518** 814–8
[5] Takase Y, Lee J W, Scheinbeim J I and Newman B A 1991 *Macromolecules* **24** 6644–52
[6] Capsal J F, Dantras E, Dandurand J and Lacabanne C 2010 *Polymer* **51** 4606–10
[7] Giacometti J A, Leal Ferreira G F and Gross B 1988 *ISE6 Proc. 6th Int. Symp. of Electrets (Oxford, UK)* pp 87–91
[8] Tasaka S, Kawaguchi M and Inagaki N 1998 *Eur. Polym. J.* **34** 1743–5
[9] Roberts S 1947 *Phys. Rev.* **71** 890–5
[10] Perls T A, Diesel T J and Dobrov W I 1958 *J. Appl. Phys.* **29** 1297–302
[11] Ibos L 2000 Contribution à l'étude de la pyroélectricité dans les polymères ferroélectriques pour capteurs integrés *PhD Thesis* Université de Toulouse
[12] Teyssedre G, Bernes A and Lacabanne C 1993 *Thermochim. Acta* **226** 65–75
[13] Wenger M P and Das-Gupta D K 1999 *Polym. Eng. Sci.* **39** 1176–88
[14] Cross L E 1995 *Jpn. J. Appl. Phys.* **34** 2525–32
[15] Capsal J F, Pousserot C, Dantras E, Dandurand J and Lacabanne C 2010 *Polymer* **51** 5207–11
[16] Wenger M P, Almeida P L, Blanas P, Shuford R J and Das-Gupta D K 1999 *Polym. Eng. Sci.* **39** 483–92
[17] Jinhua L, Ningyi Y and Chan H L W 2002 *Sensors Actuators* A **100** 231–5
[18] Furukawa T, Fujino K and Fukada E 1976 *Japan. J. Appl. Phys.* **15** 2119–29
[19] Hanner K A, Safari A, Newnham R E and Runt J 1989 *Ferroelectrics* **100** 255–60
[20] Newnham R E, Skinner D P and Cross L E 1978 *Mater. Res. Bull.* **13** 525–36
[21] Capsal J F, Dantras E, Laffont-Dantras L, Dandurand J and Lacabanne C 2010 *J. Non-Cryst. Solids* **356** 629–34
[22] Capsal J F, Dantras E, Dandurand J and Lacabanne C 2007 *J. Non-Cryst. Solids* **353** 4437–42
[23] Rao C N R, Deepak F L, Gundiah G and Govindaraj A 2003 *Prog. Solid State Chem.* **31** 5–145
[24] Marinkovic B A, Jardim P M, Morgado E Jr, de Abreu M A S, Moure G T and Rizzo F 2008 *Mater. Res. Bull.* **43** 1562–72
[25] Yuh J, Nino J C and Sigmund W M 2005 *Mater. Lett.* **59** 3645–7
[26] Fu C, Cai W, Zhou L, Chen H and Liu Z 2009 *Appl. Surf. Sci.* **255** 9444–6
[27] Joshi U A, Yoon S, Baik S and Lee J S 2006 *J. Phys. Chem.* B **110** 12249–56
[28] Joshi U A and Lee J S 2005 *Small* **1** 1172–6
[29] Xu C Y, Zhang Q, Zhang H, Zhen L, Tang J and Qin L C 2005 *J. Am. Chem. Soc.* **127** 11584–5
[30] Feenstra J and Sodano H A 2008 *J. Appl. Phys.* **103** 124108
[31] Tang H, Lin Y, Andrews C and Sodano H A 2011 *Nanotechnology* **22** 015702
[32] Andrews C, Lin Y and Sodano H A 2010 *Smart Mater. Struct.* **19** 025018
[33] Reznitchenko L A, Turik A V, Kuznetsova E M and Sakhnenko V P 2001 *J. Phys.: Condens. Matter* **13** 3875–81
[34] Zhu H, Zheng Z, Gao X, Huang Y, Martens W and Frost R 2006 *J. Am. Chem. Soc.* **128** 2373–84
[35] Maxwell Garnett J C 1905 *Phil. Trans. R. Soc. (London Ser.)* A **203** 385–420
[36] Wada T, Tsuji K and Saito T 2003 *Japan. J. Appl. Phys.* **42** 6110–4
[37] Shirane G, Newnham R and Pepinsky R 1954 *Phys. Rev.* **96** 581–8
[38] Furukawa T, Ishida K and Fukada E 1979 *J. Appl. Phys.* **50** 4904–12
[39] Li K, Wang H and Ding A 2010 *Polym. Sci. Series* B **52** 438–42